Preprint typeset using LaTeX style emulateapj v. 5/2/11

arXiv:1412.0627v1 [astro-ph.SR] 1 Dec 2014

THE TEMPERATURE DISTRIBUTION OF HORIZONTAL BRANCH STARS: METHODS AND FIRST RESULTS.[1]

E. P. Lagioia[2], E. Dalessandro[2], F. R. Ferraro[2], M. Salaris[3], B. Lanzoni[2], A. Pietrinferni[4], S. Cassisi[4]

ABSTRACT

As part of a large project aimed at characterizing the ultraviolet (UV) properties of globular clusters, we present here a theoretical and observational analysis aimed at setting the framework for the determination of horizontal branch (HB) temperature distributions. Indeed this is a crucial information to understand the physical parameters shaping the HB morphology in globular clusters and to interpret the UV emission from unresolved stellar systems. We found that the use of zero age HB color - $T_{\rm eff}$ relations is a robust way to derive effective temperatures of individual HB stars. We investigated the most suitable colors for temperature estimates, and the effect on the color - $T_{\rm eff}$ relations of variations of the initial chemical composition, and of the evolution off the zero age horizontal branch. As a test case, we applied our color - $T_{\rm eff}$ calibrations to the Galactic globular cluster M15. The photometry of M15 has been obtained with the Wide Field and Planetary Camera 2 on board the *HST*. The HB of M15 turned out to have a multimodal distribution, with a main component peaked at $T_{\rm eff} \sim 8,000$ K and confined below $T_{\rm eff} \sim 10,000$ K. The second component is peaked at $T_{\rm eff} \sim 14,000$ K and extends up to $T_{\rm eff} \sim 20,000$ K. The vast majority ($\sim 95\%$) of the HB stars in M15 is below 20,000 K, in agreement with the lack of a well populated extreme HB observed in other metal-poor globular clusters. We also verified that the temperatures derived with our analysis are consistent with spectroscopic estimates available in the literature.

Subject headings: globular clusters: general — globular clusters: individual (M15 NGC 7078) — stars: evolution

1. INTRODUCTION

The ultraviolet (UV) flux of old stellar systems like Galactic globular clusters (GGCs) is dominated by a minority of objects. Amongst them, blue Horizontal Branch (BHB) stars and their progeny, like post-early Asymptotic Giant Branch (post-EAGB) or AGB-manqué stars, are the strongest UV emitters (Welch & Code 1972). The relative contribution of the various types of stars to the total UV emission, as well as the factors that may lead to larger or smaller populations of UV-bright stars in a cluster still remain open issues (Greggio & Renzini 1990; Castellani & Tornambe 1991; Dorman et al. 1995; Lee et al. 2002; Rich et al. 2005; Sohn et al. 2006). A complete census of hot stars in stellar populations is therefore a prerequisite for comparing evolutionary models with observations (Dalessandro et al. 2012; Schiavon et al. 2012). In this regard GGCs are of paramount importance, since they are the closest example in nature of relatively simple systems and span a large range in metallicity, a small range in age and perhaps a range in helium abundance. Moreover, being typically populated by some 10^5 stars, even short-lived evolutionary phases can be properly sampled. GGCs can therefore be used to test stellar evolution models, one of the basic ingredients for the interpretation of the integrated light from distant galaxies.

Our ability to predict the fractions of UV emitters in clusters is deeply linked to understanding the physical mechanisms driving the Horizontal Branch (HB) morphology. It is commonly accepted that metallicity is the first parameter affecting the HB morphology: metal-rich GGCs typically have red HBs, while metal-poor ones have more extended and bluer HBs. However, there are several clusters with the same metallicity showing remarkable differences in HB morphology. Therefore, metallicity alone is not able to explain the complex HB zoology in GGCs (Freeman & Norris 1981). This issue, known as the "2nd parameter problem", has attracted the attention of several authors in the last decades (Sandage & Wildey 1967; van den Bergh 1967; Fusi Pecci et al. 1993; Lee et al. 1994; Catelan 2009; Dotter et al. 2010; Gratton et al. 2010; Milone et al. 2014). Although there is a general consensus about the fact that age is the main *global* 2nd parameter, i.e. a parameter that varies from cluster to cluster (Dotter et al. 2010; Gratton et al. 2010), no combination of metallicity and age can fully account for the different HB morphology observed in several GGCs. In this sense a clear example is given by the clusters M3, M13, M79 and M80 (Ferraro et al. 1997b, 1998; Dalessandro et al. 2013a). The necessity of an additional parameter was recently advised by Dotter et al. (2010) and Gratton et al. (2010; see also D'Antona et al. 2005; Dalessandro et al. 2011, 2013a; Milone et al. 2014) who suggested the cluster density (see also Fusi Pecci et al. 1993) and an internal spread of He abundance, respectively, as possible HB third parameters[5], that vary among differ-

[1] Based on on observations with the NASA / ESA *HST*, obtained at the Space Telescope Science Institute, which is operated by AURA, Inc., under NASA contract NAS5-26555.

[2] Dipartimento di Fisica e Astronomia, Università degli Studi di Bologna, via Ranzani 1, I-40126, Bologna, Italy; email: edoardo.lagioia2@unibo.it

[3] Astrophysics Research Institute, Liverpool John Moores University, IC2 Liverpool Science Park, 146 Brownlow Hill, L3 5RF, Liverpool, UK

[4] INAF - Osservatorio Astronomico di Collurania, via Mentore Maggini, I-64100, Teramo, Italy

[5] It is important to recall that also mass loss efficiency along the Red Giant Branch (RGB) plays a crucial role in determining the

ent sub-populations within the same cluster. Indeed Dalessandro et al. (2011; see also D'Antona et al. 2005) have been able to reproduce the complex HB morphology of the massive GGC NGC 2808 by assuming different He abundances for the three sub-populations revealed by photometric (Piotto et al. 2007) and spectroscopic (Bragaglia et al. 2010; Pasquini et al. 2011) analyzes. In addition, Dalessandro et al. (2013a) have shown that variations in the He abundance can account for the differences observed among M3, M13 and M79.

The typical approach to the study the HB morphology is to make use of parameters related to physical properties of HB stars (Ferraro & Paresce 1993; Fusi Pecci et al. 1993; Lee et al. 1994; Buonanno et al. 1997; Dotter et al. 2010; Milone et al. 2014). The effective temperature distribution of HB stars is the most efficient way to describe the HB morphology. It can be used to constrain the parameters driving the HB morphology in globular clusters thus shedding new light on our present understanding of the "2nd parameter problem". In addition the temperature distribution of HB stars is a prime ingredient to interpret the UV emission from unresolved stellar systems. The HB star effective temperature distribution has been studied in GGCs by means of optical data (e.g., Recio-Blanco et al. 2006; Moni Bidin et al. 2012; Salgado et al. 2013). However, in the optical and for $T_{\rm eff} > 12,000$ - 15,000 K, HB stars get increasingly faint and describe an almost vertical sequence (at approximately constant colors) because of the strong increase of the bolometric corrections with $T_{\rm eff}$. This makes color variations weakly sensitive to changes in temperature (a change of a few tenths in color corresponds to a variation of several thousands degrees in $T_{\rm eff}$). Indeed, for GGCs with extremely BHBs, effective temperatures derived from optical color-magnitude diagrams (CMDs) can be underestimated by up to $\sim 10,000$ K, as shown in the spectroscopic (Möhler et al. 2004) and photometric (Dalessandro et al. 2011) analysis of the HB temperature distribution of NGC2808.

To overcome this problem, we have surveyed 31 GGCs spanning a wide range of metallicities, mass and structural parameters with the Wide Field and Planetary Camera 2 (WFPC2) on board the Hubble Space Telescope (*HST*), by using a combination of UV and optical filters (Prop. 11975, PI: Ferraro). This dataset is ideal to characterize the properties of exotic objects in GGCs (Ferraro et al. 2001, 2009) and indeed some results from this survey aimed mainly at characterizing the properties of Blue Straggler Stars (BSSs) have been recently published (Contreras Ramos et al. 2012; Ferraro et al. 2012; Sanna et al. 2012; Dalessandro et al. 2014; Sanna et al. 2014). With only a few exceptions, all target clusters have been observed in the F170W, F255W, F336W and F555W bands. This filter setup allows us to derive temperatures in the most appropriate CMD over the entire extension of the HB. The dataset is also complemented with observations collected during the last 20 years by our group with the same camera (Ferraro et al. 1997a,b, 1998, 2003; Lanzoni et al. 2007a,b,c; Dalessandro et al. 2008a, 2011, 2013a,b).

mass of the star along the Zero Age Horizontal Branch (ZAHB), with a clear impact on the HB morphology (see Catelan 2000; Origlia et al. 2007, 2014).

In this work we first introduce our methodology to determine the $T_{\rm eff}$ distribution along the HB of our sample of GGCs, and discuss several possible sources of systematic errors.

We derive here the $T_{\rm eff}$ distribution of HB stars in the massive GGC NGC 7078 (M15). Methods and results presented in this work will be used in the following papers of the series. We note that we chose this cluster as test case for our methods because it is the only target of the entire sample with a blue HB observed in the two far UV filters, namely F160BW and F170W. This will allow us to make an homogeneous comparison with previous results obtained only in the F160BW filter (Ferraro et al. 1998; Dalessandro et al. 2011, 2013a).

In §2 we describe the approach used for the $T_{\rm eff}$ estimate. §3 describes the observations and data reduction procedures. In §4 we report the criteria adopted for the HB stars selection. In §5 the HB temperature distributions is derived. §5 summarizes the main results.

2. DERIVATION OF THE EFFECTIVE TEMPERATURES

Our methodology to determine the $T_{\rm eff}$ distribution of the observed HB stars is very similar to what employed in the study of NGC 2808 HB by Dalessandro et al. (2011). We consider the observed colors of each individual HB star in a given cluster, and derive the $T_{\rm eff}$ by interpolating a cubic spline along the color - $T_{\rm eff}$ relation given by the appropriate theoretical ZAHB, suitably reddened according to the cluster estimated extinction. This approach neglects the post-ZAHB evolutionary effects on the color - $T_{\rm eff}$ relation, that we will assess later in this section.

We have employed the BaSTI [6] α-enhanced models by Pietrinferni et al. (2006); to account for the effect of radiative levitation in the stellar atmospheres, that sets in at about 11,500 - 12,000 K (see for example Pace et al. 2006), we have applied bolometric corrections appropriate for [Fe/H]=0.0 and scaled-solar mixture to the HB models, when $T_{\rm eff}$ is above 12,000 K [7]. While this is a crude approximation (made necessary by the lack of more suitable complete grids of HB stellar evolution and atmosphere models), it still provides reliable measures of the temperatures when compared to spectroscopic estimates for hot HB stars (see discussion in Dalessandro et al. 2011). Remarkably, we found that the color - $T_{\rm eff}$ relation of our chosen filter combinations (but not the individual magnitudes), is practically identical to the counterpart obtained from ZAHB models with the same composition but without the recipe to mimic the effect of radiative levitation above 12,000 K. Figure 1 displays the ZAHB color - $T_{\rm eff}$ relations for five filter combinations (employing the filters available from our observations) with sufficiently large baseline and different metallicities. The effect of the metals is visible only below $\sim 8,000$ K, mainly for $(m_{\rm F255W} - m_{\rm F555W})$ and for the redder filter combinations that we are not going to use in our analysis (see below). Moreover, the differences shown in Fig. 1 are upper limits, since they are obtained for extremely different metallicities. Our model grid allows us to pick

[6] http://basti.oa-teramo.inaf.it/index.html

[7] We tested the use of a super-solar abundance, i.e. [Fe/H] = +0.5, for the bolometric corrections at $T_{\rm eff}$ larger than 12,000K and we found no appreciable difference in the resulting color - $T_{\rm eff}$ relation.

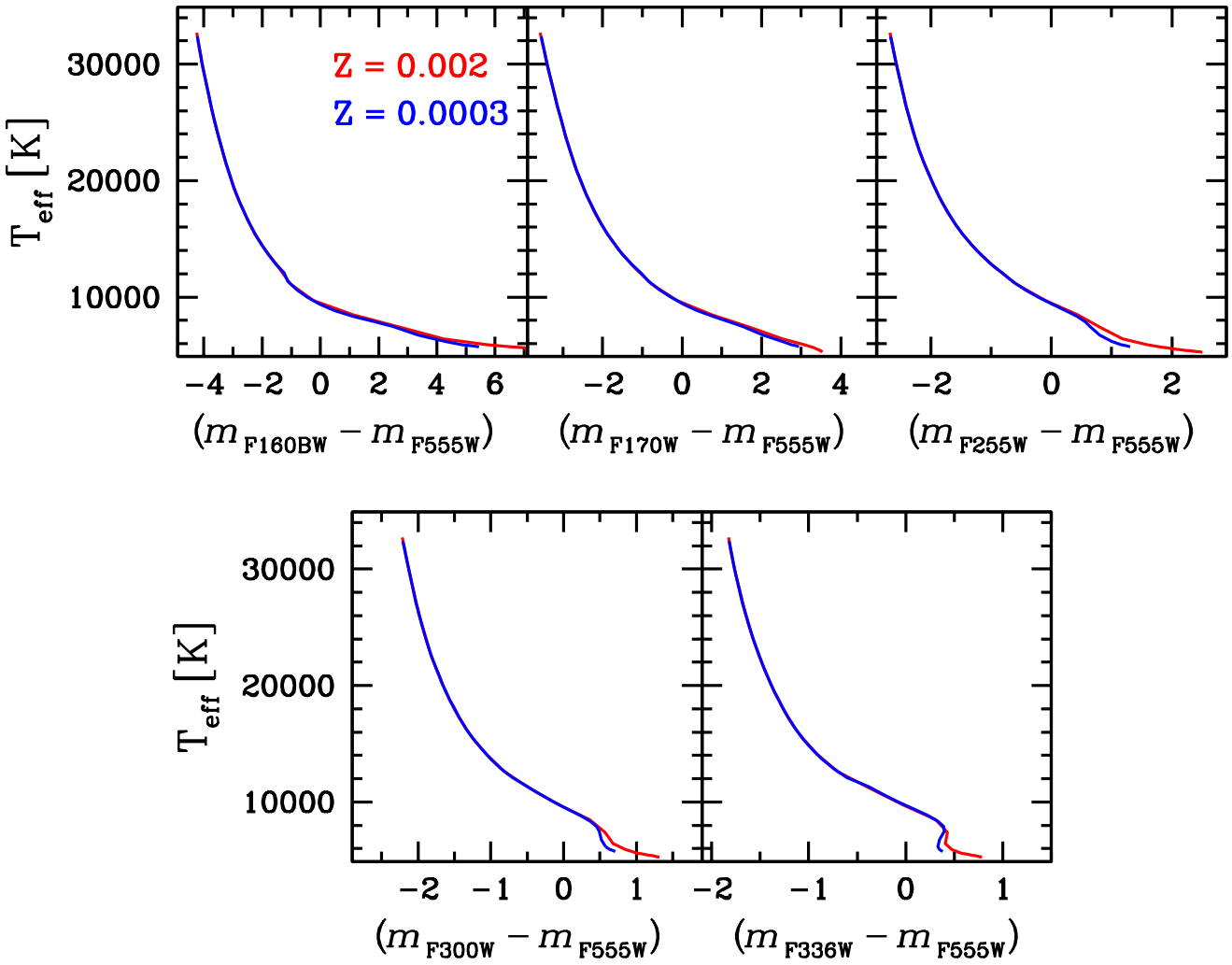

Figure 1. Color - T_{eff} relations from ZAHB models for several color combinations obtained from our photometry, and two different metallicities (see text for details).

ZAHB sequences with a metallicity within less than a factor of two of the estimates for each surveyed cluster, and therefore the related uncertainty on the individual T_{eff} values below 8,000 K is always kept below ~ 100 K. We can conclude that metallicity does not play a major in the determination of the color - T_{eff} relations.

It becomes also clear from Fig. 1 that the $(m_{F170W} - m_{F555W})$ and $(m_{F160W} - m_{F555W})$ colors are the most sensitive to T_{eff} variations (they span a larger range for the same T_{eff} interval) at any regime. However, the individual m_{F160BW} and m_{F170W} magnitudes become very faint for $T_{eff} < 10,000$ K , and our photometry in these filters can be severely incomplete. The second best choice for temperature determination below 10,000 K is $(m_{F255W} - m_{F555W})$; the color range is almost halved, but the completeness of our data is much more reliable. Therefore this is our selected color for this temperature range. Redder filter combinations are less suited for T_{eff} determinations, and the $(m_{F336W} - m_{F555W})$ color is almost insensitive to T_{eff} below $\sim 8,000$ K.

Given that it is now well known that stars within individual clusters can cover a non negligible range of He abundances (see e.g. D'Antona et al. 2005; Dalessandro et al. 2011; Milone et al. 2014 and references therein) we have analyzed the impact of Y variations on the ZAHB color - T_{eff} relations. In particular, Figure 2 displays the effect of two different initial He mass fractions (Y = 0.245 and Y = 0.300) on the predicted ZAHB color - T_{eff} relations for the filter combinations we are going to use in our investigations. It emerges clearly that the effect of the in principle unknown Y content of the observed stars is completely negligible at any T_{eff}. Another factor that may affect the relation is the fact that stars along the observed HB are born with different patterns of CNONa abundances. In Dalessandro et al. (2013a; see appendix A) we have al-

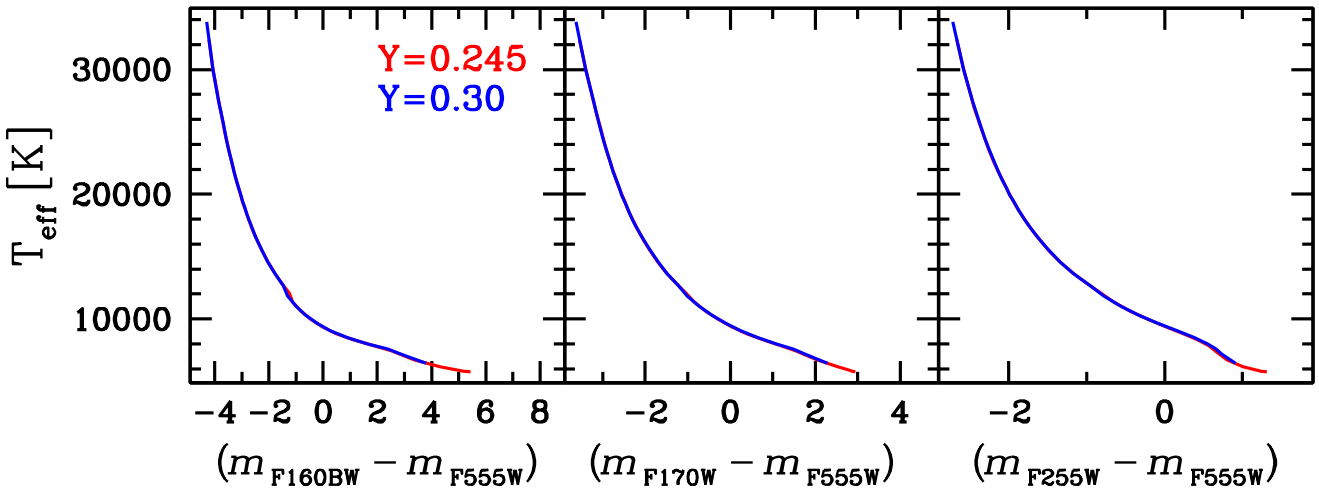

Figure 2. As Fig. 1 but for the effect of the initial He mass fraction Y, for the three colors we will use in our study (see text for details).

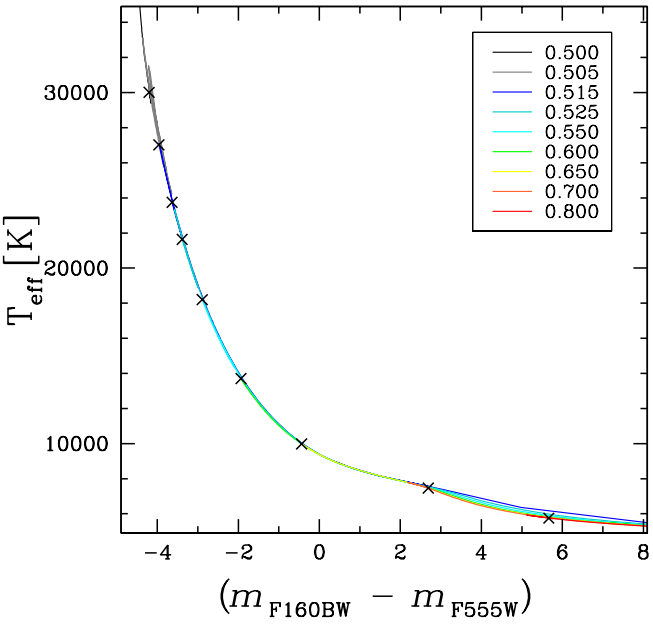

Figure 3. As Fig. 1 but for the $(m_{\rm F160W} - m_{\rm F555W})$ - $T_{\rm eff}$ relations obtained from HB tracks of different masses, with Z = 0.0003 and Y = 0.245. Crosses mark the ZAHB location of each displayed track (see text for details).

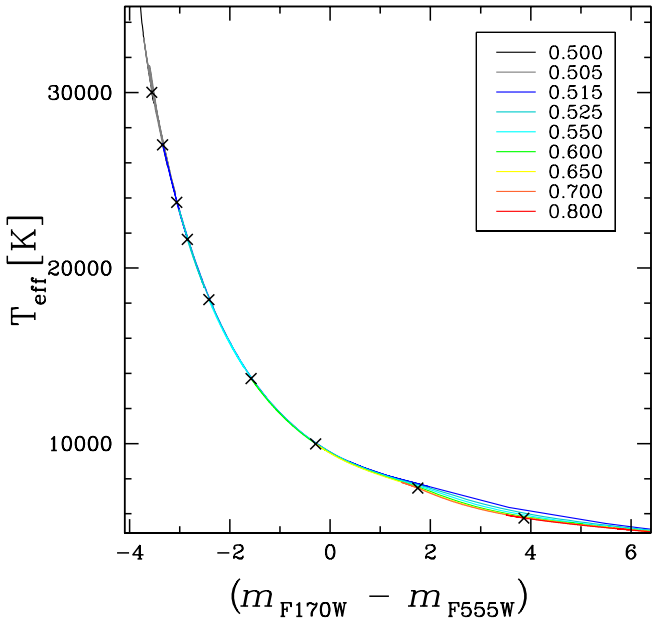

Figure 4. As Fig. 3 but for the $(m_{\rm F170W} - m_{\rm F555W})$ - $T_{\rm eff}$ relations.

ready shown that also the effect of the CNONa anticorrelations is negligible.

After having established the filter combinations to use for our $T_{\rm eff}$ estimates, and assessed the effect of the chosen initial chemical composition of the ZAHB, we address here the issue of the effect of surface gravity. We recall that we apply a color - $T_{\rm eff}$ relation obtained from the ZAHB to the observed color of HB stars, irrespective of whether they are evolving close to the ZAHB or are evolved off-ZAHB. To assess the extent of systematic biases introduced by this procedure, Figures 3, 4 and 5 display the relevant color - $T_{\rm eff}$ relations for HB tracks of different masses and the same initial chemical composition (Z = 0.0003, Y = 0.245). For the $(m_{\rm F160W} - m_{\rm F555W})$ and $(m_{\rm F170W} - m_{\rm F555W})$ colors the effect of off-ZAHB evolution is negligible at all $T_{\rm eff}$ covered by the models. In fact, in the color - $T_{\rm eff}$ diagram the off-ZAHB evolution of the models nicely overlaps with the ZAHB sequence. The effect is small also for $T_{\rm eff} < 8,000$ K, but, as anticipated, we are not going to use these colors combinations for red HB stars. Also for the $(m_{\rm F255W} - m_{\rm F555W})$ color diagram evolutionary effects are in general negligible. However they start to be visible below $\sim 8,000$ K. The maximum effect is at $T_{\rm eff}$ in the range between $\sim 6,000$ and 7,500 K and amounts to $\sim 1,000$ K. This represents the maximum systematic error due to evolutionary effects for our individual temperature estimates below 10,000 K.

As discussed in detail by Girardi et al. (2008) the extinction coefficients for broadband filters may depend on the effective temperature of the stars. If this is the case,

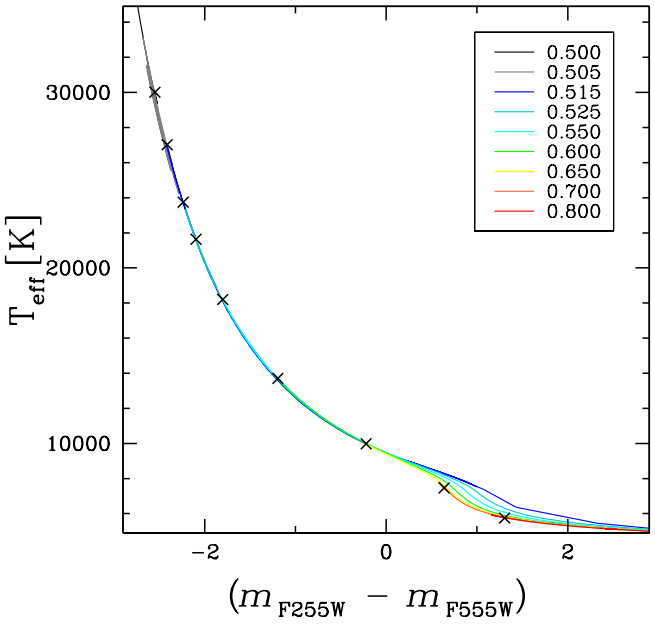

Figure 5. As Fig. 3 but for the $m_{F255W} - m_{F555W}$ - T_{eff} relations.

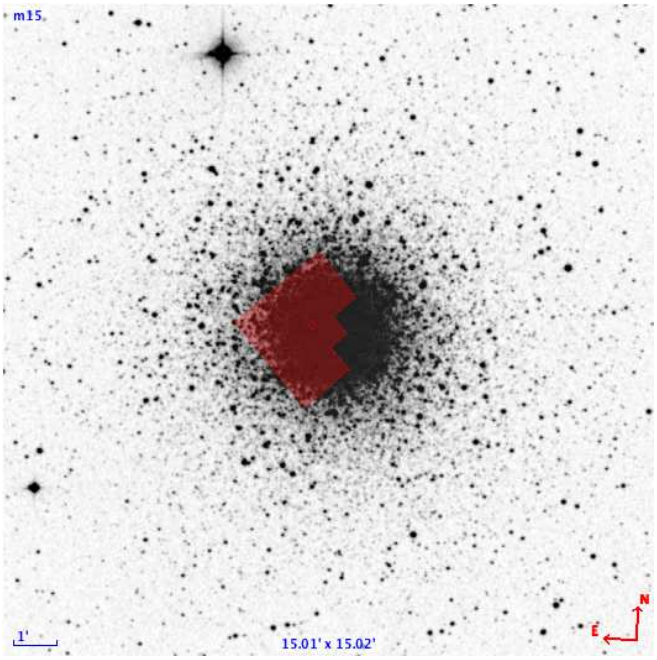

Figure 6. Footprint of the WFPC2 images used in this work, superimposed on a 15′ × 15′ DSS POSS-I plate. North is up and East is left.

Table 1
WFPC2 images of M15 used in this work.

Filter	No. of images × Exp. time (sec)
F160BW	1×1500
F170W	$1 \times 1000 + 3 \times 700$
F255W	3×1200
F300W	$1 \times 80 + 3 \times 600$
F336W	$1 \times 40 + 1 \times 700 + 2 \times 800$
F555W	$1 \times 1 + 3 \times 40$

the theoretical color - T_{eff} relations should be modified to take this into account when applied to the cluster HB stars. Following the methods outlined in Girardi et al. (2008) we have verified that for the F170W filter and $T_{eff} > 10,000$ K, the extinction displays a negligible dependence on the temperature, and the same is true for the F255W filter when $T_{eff} < 10,000$ K. This guarantees that the slopes of the color - T_{eff} relations that we use do not depend on the individual values of $E(B-V)$.

Finally, for the very rare cases (in our sample) of clusters hosting blue-hook stars, which are hotter than the bluest end of any ZAHB, we will use hot-flashers models as already done for NGC 2808 (Dalessandro et al. 2011).

3. OBSERVATIONS AND DATA REDUCTION

The dataset used in this work consists of 20 WFPC2 images collected on Apr 16th 2009 and centered on the core of M15, as shown in Figure 6. Table 1 summarizes filters and exposure times of the observations.

All the images have been pre-processed through the standard *HST*/WFPC2 pipeline for bias - dark subtraction and flat fielding. They have been corrected also for the pixel area and '34th row' effect, which are specific instrument-induced signal variations (Baggett et al. 2002). Single frames were extracted from the WFPC2 mosaic image and, for each given chip and filter, we combined them with the IRAF [8] task `imcombine`, applying a cosmic-ray rejection algorithm.

The photometric analysis was performed both on raw and median images, by means of the DAOPHOT IV/ALLSTAR suite (Stetson 1987). We first obtained preliminary catalogs independently for each frame by using the DAOPHOT star-finding algorithm. Then, we built up an initial common list of identifications by geometrically matching, with DAOMATCH/DAOMASTER (Stetson 1993), these preliminary catalogs.

Cross-identifications are assumed to be real detections if they occur in at least a minimum number of frames which varies from filter to filter. This step is aimed at discarding possible spurious cosmic-ray detections survived on the median image as well as fake detections from the preliminary catalogs of the raw images. Since we have only one exposure in the F160BW filter, a reliable star list in this band has been obtained after cross-matching the preliminary F160BW catalog with those derived in F170W.

Once obtained a reliable common list of objects, we estimated a suitable point spread function (PSF) on the median image through the selection of bright and isolated stars uniformly distributed over the entire chip area. Given the stability of the *HST* PSF, and since the S/N of the median is higher than that of the single image, we applied the PSF model obtained for the former to the latter. We assumed a quadratic variation of the PSF with the position on the frame for all the images but the F160BW and F170W ones, where the limited number of stars restricted our choice to a linearly variable PSF model.

[8] IRAF (Image Reduction and Analysis Facility) is distributed by the National Optical Astronomy Observatory, which is operated by the Association of Universities for Research in Astronomy, Inc., under cooperative agreement with the National Science Foundation.

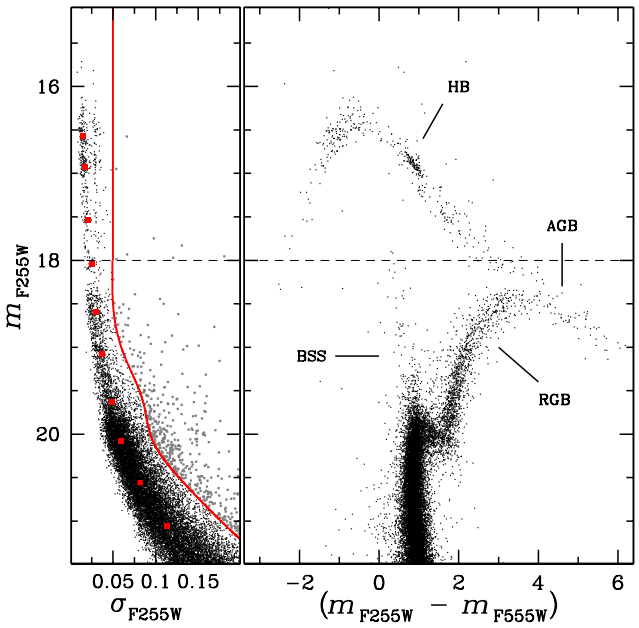

Figure 7. *Left*: Plot of magnitude *vs.* standard error of magnitude in the F255W band. The red squares mark the median point in each 0.5 mag bin. The red solid line divides 'well-measured' (black dots) and rejected (gray dots) stars. *Right*: $(m_{F255W}, m_{F255W} - m_{F555W})$ CMD of the well-measured stars. The different evolutionary branches have been labeled.

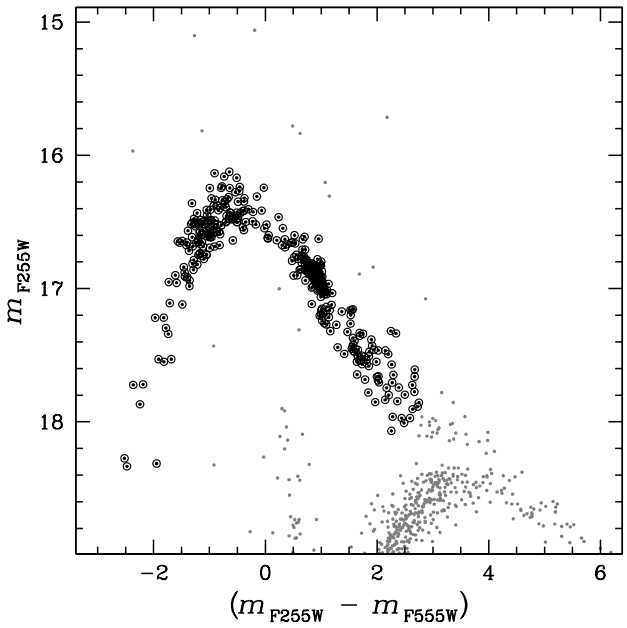

Figure 8. Zoom of the HB region in the $(m_{F255W}, m_{F255W} - m_{F555W})$ CMD of M15. Black circles represent the final selection of HB members.

For each chip we created two master lists: the first includes stars detected in at least two median images among those obtained in the F255W, F300W, F336W and F555W filters, after they have been transformed to a common reference system; the second includes stars detected in at least two F170W exposures. Stars in the master lists were then forced to fit in single images with ALLFRAME (Stetson 1994), separately for each filter.

Afterwards, the following quantities were computed and applied in sequence to the new instrumental catalogs:

- aperture correction within a nominal infinite aperture. It was obtained by subtracting 0.1 mag to the correction for an aperture within a radius of 0.5″ calculated with DAOGROW (Stetson 1990).
- correction for Charge Transfer Efficiency loss by means of the equations provided in Dolphin (2009);
- corrections for UV Contamination and Long-term Quantum Efficiency Change by reading the value of the ZP_CORR keyword in the file header.

3.1. *Photometric and astrometric calibration*

For each filter we matched the catalog of the single images, obtaining six different master lists, where the instrumental magnitude and the error of the magnitude are, respectively, the weighted mean of the single image measurement reported to the system of the reference frame of the transformation and the standard error of the mean, based on individual frame standard errors (Ferraro et al. 1991, 1992). Instrumental magnitudes were then transformed into the VEGAMAG system adding the zero points listed in table 5.1 of the WFPC2 Data Handbook [9] (ver.5.0, July 2010, Baggett et al. 1997). Since there is no overlap among the different WFPC2 chips, we adopted an empirical procedure to quantify the zero point variation among them (see appendix A). The final total catalog counts $\sim 44,000$ stars.

In order to transform the star instrumental pixel-based position into the absolute equatorial coordinate system we performed a two-step procedure (as already done in previous works; see for example Dalessandro et al. 2009) Firstly, we reported the instrumental WFPC2 coordinates to the reference system of the M15 ACS catalog, available in the ACS Survey of Galactic Globular Cluster Database [10] (Sarajedini et al. 2007). Secondly, we put these new coordinates onto the 2MASS Point Source Catalogue system (Cutri et al. 2003). Both steps were achieved by means of the CATAXCORR/CATACOMB package, developed by P. Montegriffo at the Bologna Astronomical Observatory (private communication). The program provided us with a very accurate astrometric solution for the transformation into the absolute system of ACS, with typical error of $\sim 0.3''$ in right ascension and declination, for stars measured in the Planetary Camera (PC) chip, (whose pointing is located at the very center of the cluster) and of $\sim 0.02''$ for the stars in the three Wide Field (WF2, WF3, WF4) cameras. The corrections to the absolute system of 2MASS were determined with an error of $\sim 0.16''$ in both the coordinates.

3.2. *Sample selection and RR Lyræ identification*

The definition of a sample of HB stars measured with high photometric accuracy is fundamental in our analysis. To this purpose, we adopted the following procedure.

[9] http://www.stsci.edu/hst/wfpc2/documents/handbook/WFPC2_DHB.html

[10] http://www.astro.ufl.edu/~ata/public_hstgc/databases.html

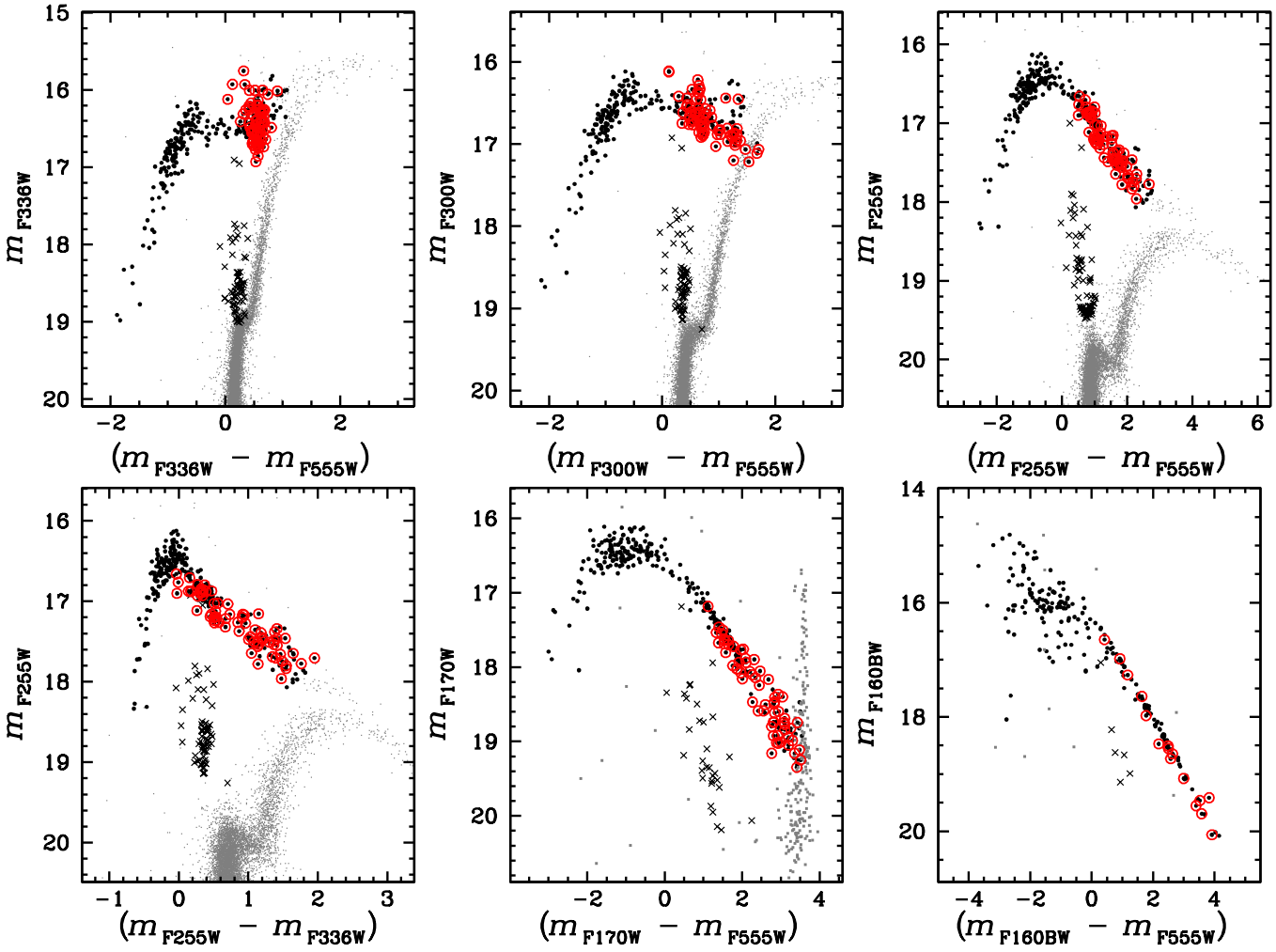

Figure 9. CMD of M15 in six different combination of filters. The various stellar components of the clusters are coded as following: gray dots = MS + SGB + RGB/AGB; black cross = BSS; black black point = HB. The RR Lyræ in common between our catalog and the Clement's *Catalogue of Variable Stars in Galactic Globular Clusters* are marked by red circles.

We first identified the RR Lyraæ in our catalog and then used the magnitude errors of the non variable stars to select the best-measured objects. Finally, we precisely identified the HB members by looking at their position in several CMDs.

For the sake of convenience, we started our selection procedure in the F255W band. Indeed, taking a look at the $(m_{\rm F255W}, m_{\rm F255W} - m_{\rm F555W})$ CMD in the right panel of Figure 7, we see that HB stars are among the brightest objects in this diagram (Ferraro et al. 2003), most of them attaining F255W magnitudes brighter than ~ 18. As expected, when plotting the magnitude error as a function of the magnitude we see a typical trend (left panel of Fig. 7): the fainter the star, the larger its error. We divided the full magnitude range into small intervals of 0.5 mag and for each one we computed the median value of the magnitude and of the error (red squares). Then, in each magnitude bin at $m_{\rm F255W} > 18$, we selected all stars with an error within 3σ from the median value and we fit the upper boundary of this error distribution with a cubic spline. An upper limit of 0.05 mag was instead adopted for stars brighter than $m_{\rm F255W} = 18$. Stars with a magnitude error smaller than the fit value were flagged as 'well-measured' (black dots). Since a similar trend for the magnitude error is found in the other bands, the same selection method was applied to the F170W, F300W, F336W and F555W magnitudes [11]. In principle only those stars satisfying the selection criterion in all the filters should be flagged as 'well-measured' objects. However, since the selection criterion in the F255W filter excludes most of the stars with uncertain measures also in other filters, in the following we consider as 'well measured' all the objects satisfying only the selection in the F255W filter. Figure 8 presents the final selection of the well measured HB stars (marked with large empty circles). As can be seen the considered sample includes the vast majority of the observed HB stars. Also visible in the figure is the brightest portion of the RGB and AGB at $(m_{\rm F255W} - m_{\rm F555W} \gtrsim 2$ and the BSS sequence at $(m_{\rm F255W} - m_{\rm F555W}) \sim 0.5$ extending up to $m_{\rm F255W} \sim 18$. With the adopted selection we may either lose a few genuine HB stars or include some post-HB objects, but they constitute only a negligible fraction of the selected sample. In fact, based on the evolutionary timescales, we expect just one post-HB star every one hun-

[11] A bin of 0.4 mag was adopted for the analysis in the F300W, F336W and F555W filters.

dred genuine HB objects (see, e.g., Schiavon et al. 2012). Figure 9, which displays the final CMDs in different band combinations, shows that the selected stars look like genuine HB objects also in the other CMDs. Moreover, the $(m_{\rm F336W}, m_{\rm F336W} - m_{\rm F555W})$ CMD demonstrates that our choice of the red boundary of the HB selection is reliable, because in that CMD, AGB stars are better separated from the HB.

In addition to the HB stars, we highlighted the position of the BSSs in all CMDs of Fig. 9. It is worth to notice that moving from pure optical $(m_{\rm F336W}, m_{\rm F555W})$ to mid UV - optical $(m_{\rm F255W}, m_{\rm F555W})$ and far UV - optical $(m_{\rm F160BW}, m_{\rm F555W})$ CMDs, the brightest and reddest stars, namely the RGBs/AGBs, become progressively fainter with respect to the BHBs and EHBs which at the contrary are the brightest objects in the $(m_{\rm F160BW}, m_{\rm F160BW} - m_{\rm F555W})$ and $(m_{\rm F170W}, m_{\rm F170W} - m_{\rm F555W})$ CMDs.

In the latter case (see bottom-middle panel of Fig. 9), we observe two specific features:

1. the RGB/AGB sequence is vertical and the reddest RGB/AGB stars are as bright as the BHBs/EHBs;
2. the reddest cluster HBs merge with the vertical RGB/AGB sequence.

Both features are caused by the particular behavior of the F170W filter. This filter is characterized by a significant *red leak* due to a tail of sensibility of the spectral response curve at long wavelengths. According to that, cool stars appear much brighter in F170W than in other UV filters (Girardi et al. 2008).

Given that RR Lyræ are observed at random phase, they have been excluded from our HB sample. M15 is known to host about 200 RR Lyræ (Corwin et al. 2008). Since our dataset is not suited for variability analysis, RR Lyræ have been observed at random phase. A list of variables is however available in the *Catalogue of Variable Stars in Galactic Globular Clusters* (Clement et al. 2001), from which we retrieved the position and classification of 168 RR Lyræ. Among them, only 82 fall in the surveyed FoV. By using cataXcorr we geometrically matched our catalog and the Clement's one, finding 72 cross-identifications. Among the stars not in common, four lie in the gaps of the WFPC2 mosaic and for the remaining six we cannot establish an unambiguous association with stars in our list. Their position in the various CMDs is shown in Figure 9.

4. TEMPERATURE DISTRIBUTION ALONG THE HB

The typical photometric error of the selected HB stars in the colors based on F170W and F255W is $\sigma \sim 0.03$, corresponding approximately to a small random error $\Delta T_{\rm eff} \sim 100\,{\rm K}$ on the individual estimates. A realistic uncertainty on the cluster reddening, $\Delta E\,(B-V)$ by 0.01-0.02 mag, would introduce a systematic error of the order of 250-500 K, that dominates compared to the random error arising from photometry. On the other hand the photometric errors in F160BW are much larger, of the order of $\sigma \sim 0.15$, corresponding to $\Delta T_{\rm eff} \sim 1,000\,{\rm K}$. As a consequence, even if in principle the $(m_{\rm F160BW} - m_{\rm F555W})$ color is well suited for our analysis, in this case it is strongly affected by the uncertainties caused by photometric errors. However, given that M15 is the only cluster for which a direct comparison between F160BW and F170W is possible, we decided to use also the F160BW band with this caveat in mind.

All the color - $T_{\rm eff}$ relations used in the following discussion have been obtained through ZAHB models with metallicity [Fe/H] $= -2.14$, which is the closest value to the metallicity of M15 ([Fe/H] $= -2.39 \pm 0.14$; Roediger et al. 2014) available in the BaSTI database, and primordial helium abundance, namely Y $= 0.245$. We adopted a reddening $E\,(B-V) = 0.10$ (Harris 1996; 2010 update) to correct the theoretical colors.

The top panel in Figure 10 displays the derived temperature distributions obtained from the $(m_{\rm F160BW} - m_{\rm F555W})$ - $T_{\rm eff}$ relation (black histogram) and $(m_{\rm F170W} - m_{\rm F555W})$ - $T_{\rm eff}$ relation (shaded histogram) for all the HB stars having a color estimate in the $(m_{\rm F160BW}, m_{\rm F160BW} - m_{\rm F555W})$ CMD. Both show a main peak located at $T_{\rm eff} \sim 8,000\,{\rm K}$ and a broad distribution extending from $\sim 10,000\,{\rm K}$ to $\sim 22,000\,{\rm K}$. The three stars hotter than $\sim 26,000\,{\rm K}$ in the $(m_{\rm F160BW} - m_{\rm F555W})$ distribution attain lower $T_{\rm eff}$ in the $(m_{\rm F170W} - m_{\rm F555W})$ temperature distribution. This offset is likely due to the large photometric errors in $(m_{\rm F160BW} - m_{\rm F555W})$, at these colors. According to the Kolmogorov-Smirnov test, the distributions of effective temperatures obtained with the two colors for $T_{\rm eff} < 22,000\,{\rm K}$ are statistically indistinguishable.

The complete temperature distribution of the HB stars of M15 is shown in the bottom panel of the Fig 10. It has been obtained through the combination of F555W with F170W magnitudes, for stars having $T_{\rm eff} > 10,000\,{\rm K}$ according to the $(m_{\rm F170W} - m_{\rm F555W})$ - $T_{\rm eff}$ relation, and through the combination of F555W with F255W magnitudes for stars having $T_{\rm eff} < 10,000\,{\rm K}$, according to the $(m_{\rm F255W} - m_{\rm F555W})$ - $T_{\rm eff}$ relation (see Sect. 2 for details). This artificial splitting of the HB sample may generate duplication or loss of a few objects. We carefully checked the final sample and we found that only three objects would have been not considered. We therefore assigned them the average value of the temperature obtained from the two color indices.

On the whole we observe a main component peaked at $\sim 8,000\,{\rm K}$ and confined below $\sim 10,000\,{\rm K}$. The second component, vaguely Gaussian is peaked at $T_{\rm eff} \sim 14,000\,{\rm K}$. Although the hottest HB star is located at 30,000 K in qualitative agreement with what found by Möhler et al. (1997) and Recio-Blanco et al. (2006), the derived distribution shows that only a few stars can be found at $T_{\rm eff} > 20,000\,{\rm K}$ (Möhler et al. 1995). This can be more easily appreciated from Figure 11, which displays the cumulative temperature distribution of the HB stars in M15 obtained before. As can be seen, essentially the 95% of the stars in the M15 HB is below $T_{\rm eff} = 20,000\,{\rm K}$.

4.1. *Comparison with spectroscopic data*

The temperature of HB stars obtained through the color - $T_{\rm eff}$ relation might be prone to systematic errors introduced by the theoretical model assumptions and the parameters (e.g. reddening) used to fit the observations . In order to validate the temperature estimates, spectroscopic temperature determinations of the same HB stars can be used.

In the case of M15, spectroscopic observations of the

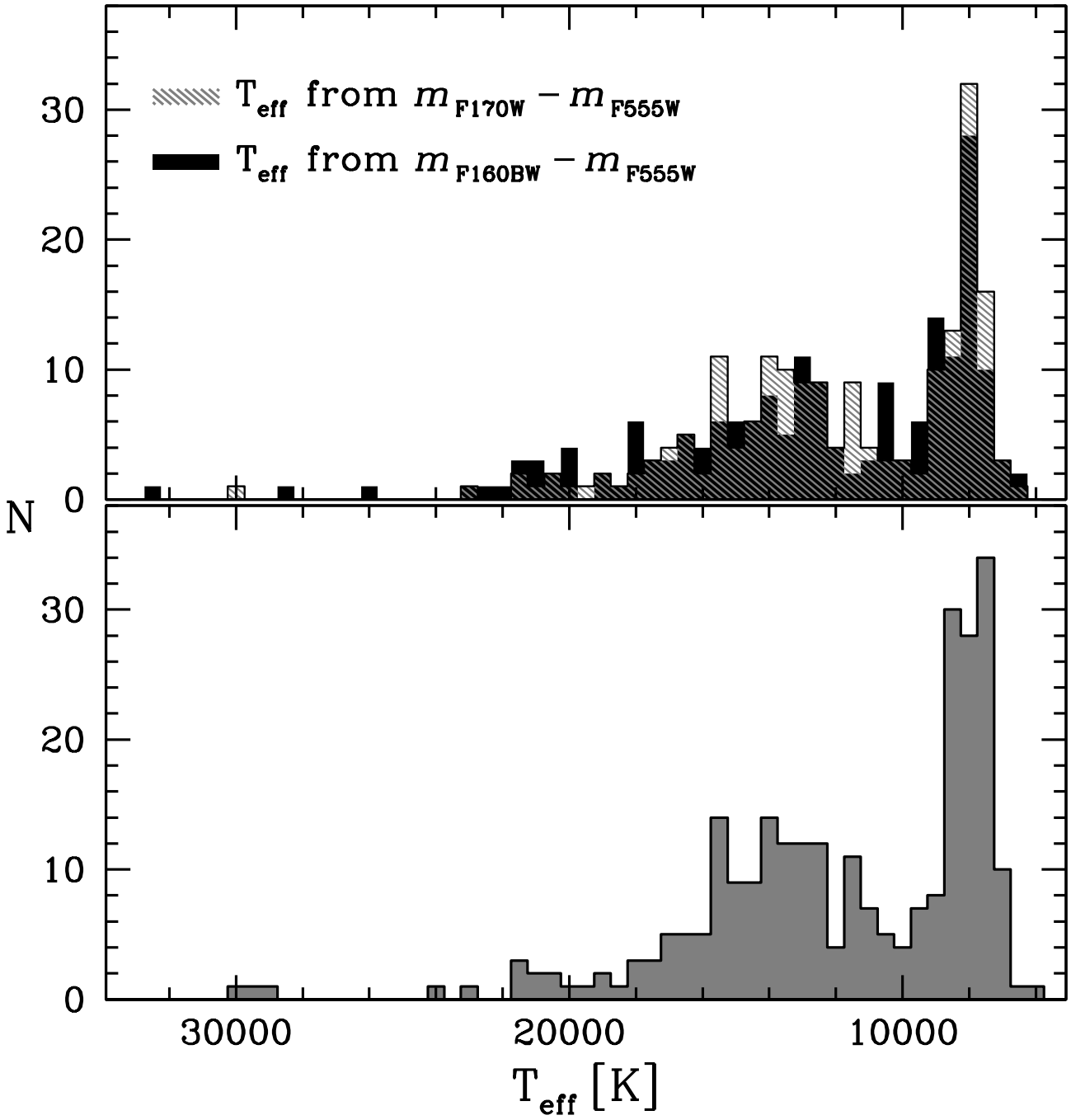

Figure 10. Top: Histograms of the temperature distribution of the HB stars in M15 obtained from the $(m_{\rm F170W} - m_{\rm F555W})$ - $T_{\rm eff}$ (solid black) and $(m_{\rm F170W} - m_{\rm F555W})$ - $T_{\rm eff}$ (gray shaded) relation for all the HB stars with a color estimate in the $(m_{\rm F160BW}, m_{\rm F160BW} - m_{\rm F555W})$ CMD. Bottom: Histogram of the temperature distribution of the HB stars in M15 obtained from the $(m_{\rm F170W} - m_{\rm F555W})$ - $T_{\rm eff}$ relation for stars with $T_{\rm eff} > 10,000\,K$, and from the $(m_{\rm F255W} - m_{\rm F555W})$ - $T_{\rm eff}$ relation for stars with $T_{\rm eff} < 10,000\,{\rm K}$ (see text for details). All the distributions have been obtained adopting a BaSTI ZAHB model with [Fe/H] = −2.14 and Y = 0.245.

cluster's HB stars were performed by Möhler et al. (1995, 1997) and by Behr (2003). The three spectroscopic samples were selected from the ground-based U, B, V catalog of Buonanno et al. (1983), which unfortunately does not overlap our FoV. Therefore, no direct comparison has been possible. However, we devised the following procedure to test the reliability of our temperature scale.

Since the photometry of Buonanno et al. (1983) is fully compatible with that of Stetson (1994) [12], we cross-matched the latter dataset with our catalog, finding 136 stars in common, 26 being HB stars, mainly populating the red portion of the branch. We used this subsample of stars in order to find a relation between the (B − V) and the $(m_{\rm F170W} - m_{\rm F555W})$ colors. This relation has been used to transform the (B − V) color of 17

[12] Available on the Peter Stetson's Photometric Standard Fields website: http://www3.cadc-ccda.hia-iha.nrc-cnrc.gc.ca/community/STETSON/standards/

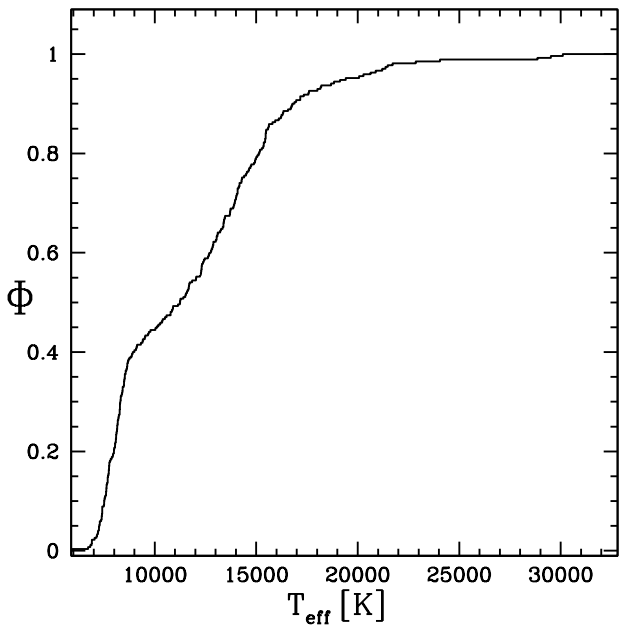

Figure 11. Cumulative temperature distribution for the HB stars of M15 obtained from the $(m_{\rm F170W} - m_{\rm F555W})$ - $T_{\rm eff}$ relation and adopting an α-enhanced ZAHB model with [Fe/H] = −2.14 and Y = 0.245.

stars measured by Behr (2003) and 6 stars observed by Möhler et al. (1995), in the UV color and then in temperature. This finally allowed us to compare the temperatures obtained from the ZAHB colors with those obtained from the spectroscopy. The results are shown in Figure 12. The top panel shows the difference between the spectroscopic temperature estimates and the temperatures extracted from the color - $T_{\rm eff}$ relation of the adopted ZAHB model (see Sect. 4). We found a median difference of $\approx -600 \pm 20$ K, both below and above 10,000 K. Such a difference is comparable to the average precision of our HB temperature estimates. Although the difference is systematic, it can be easily explained by just a 0.02 mag overstimate of the cluster reddening (see Sect. 4). Note that one star (B348 in Buonanno et al. 1983) is in common between the two spectroscopic catalogs. Interestingly the difference between the two spectroscopic temperatures ($\sim$ 400 K) is similar to the difference with respect to our photometric measures (see the two filled symbols in Fig. 12). In the lower panel of Fig. 12 the absolute value of the relative difference is plotted: all the stars scatter around $|\Delta T/T| = 0.05$ with only three objects above 0.10. The results of this comparison clearly confirms the reliability of our approach.

5. SUMMARY AND CONCLUSIONS

This work is part of a series of papers that aims at studying the temperature distribution of a large sample of GGCs, for which we obtained homogeneous UV and optical *HST* data.

The temperature is derived by using the ZAHB color - $T_{\rm eff}$ relations by Pietrinferni et al. (2006). We investigated here the most suitable colors for temperature estimates, the effect of metallicity variations, the impact of neglecting off-ZAHB evolution and also the impact of neglecting differences of He abundances among HB stars on the adopted color - $T_{\rm eff}$ relations.

As already shown by Rood et al. (2008) and Dalessandro et al. (2011, 2013a) we found that the $(m_{\rm F160BW} - m_{\rm F555W})$ and $(m_{\rm F170W} - m_{\rm F555W})$ color combinations are most sensitive to $T_{\rm eff}$ variations. However since the sample of red HB stars can be partially incomplete in far-UV bands for some clusters, the use of the $(m_{\rm F255W} - m_{\rm F555W})$ can be considered as a good alternative choice at $T_{\rm eff} < 10,000$ K. We have shown that variations in metallicity and He have a negligible effect on the ZAHB color - $T_{\rm eff}$ relations. Moreover we have found that also the effect of gravity due to the off-ZAHB evolution of HB stars has an almost negligible effect in any color combination for $T_{\rm eff} > 8,000$ K, while at lower temperatures in the $(m_{\rm F255W} - m_{\rm F555W})$ color, it introduces a maximum systematic error of $\sim 15\%$ on individual temperatures. These results fully justify the use of the ZAHB color - $T_{\rm eff}$ relations.

As a test case in our analysis, we have applied our approach to the metal poor GGC M15. We performed a photometric analysis of 20 images centered on the core of the cluster, collected in the filters F160BW, F170W, F255W, F300W, F336W and F555W. Since M15 is the only cluster in our survey for which we have a total filter coverage, it serves as calibrator for our database.

We derived the temperature of M15 HB stars by using the theoretical color - $T_{\rm eff}$ relation for [Fe/H] = −2.14. We compared the temperature distributions from the $(m_{\rm F160BW} - m_{\rm F555W})$ and $(m_{\rm F170W} - m_{\rm F555W})$ colors, finding a good agreement between the two. This outcome enables a direct comparison with results already published by our group for clusters with only F160BW observations. However, since the other clusters in our sample have been observed only in the F170W filter, we adopted the temperature distribution obtained from the $(m_{\rm F170W} - m_{\rm F555W})$ - $T_{\rm eff}$ relation. Moreover, we adopted the temperatures obtained by the $(m_{\rm F255W} - m_{\rm F555W})$ - $T_{\rm eff}$ for $T_{\rm eff} < 10,000$ K because the completeness of our data is higher in the F255W band for relatively cold stars.

The temperature distribution of the HB stars in M15 is clearly multimodal with a main component peaked at $\sim 8,000$ K and confined below 10,000 K. The second component is peaked at $T_{\rm eff} \sim 14,000$ K and it extends up to $T_{\rm eff} \sim 20,000$ K. Indeed even if the hottest HB star in M15 has been found at $T_{\rm eff} \sim 30,000$ K, in agreement with Recio-Blanco et al. (2006) and Möhler et al. (1995), it is important to emphasize that 95% of the HB population in M15 lies below $T_{\rm eff} \sim 20,000$ K. We have also shown that the temperature estimates obtained from ZAHB colors are consistent with previous spectroscopic estimates (Möhler et al. 1995; Behr 2003).

This research is part of the project COSMIC-LAB (http://www.cosmic-lab.eu) funded by the European Research Council (under contract ERC-2010-AdG-267675).

REFERENCES

Baggett, S., Casertano, S., Gonzaga, S., & Ritchie, C. 1997, Space Telescope WFPC2 Instrument Science Report, 10
Baggett, S., et al. 2002, in *HST* WFPC2 Data Handbook, v. 4.0, ed. B. Mobasher, Baltimore, STScI
Behr, B. B. 2003, ApJS, 149, 67

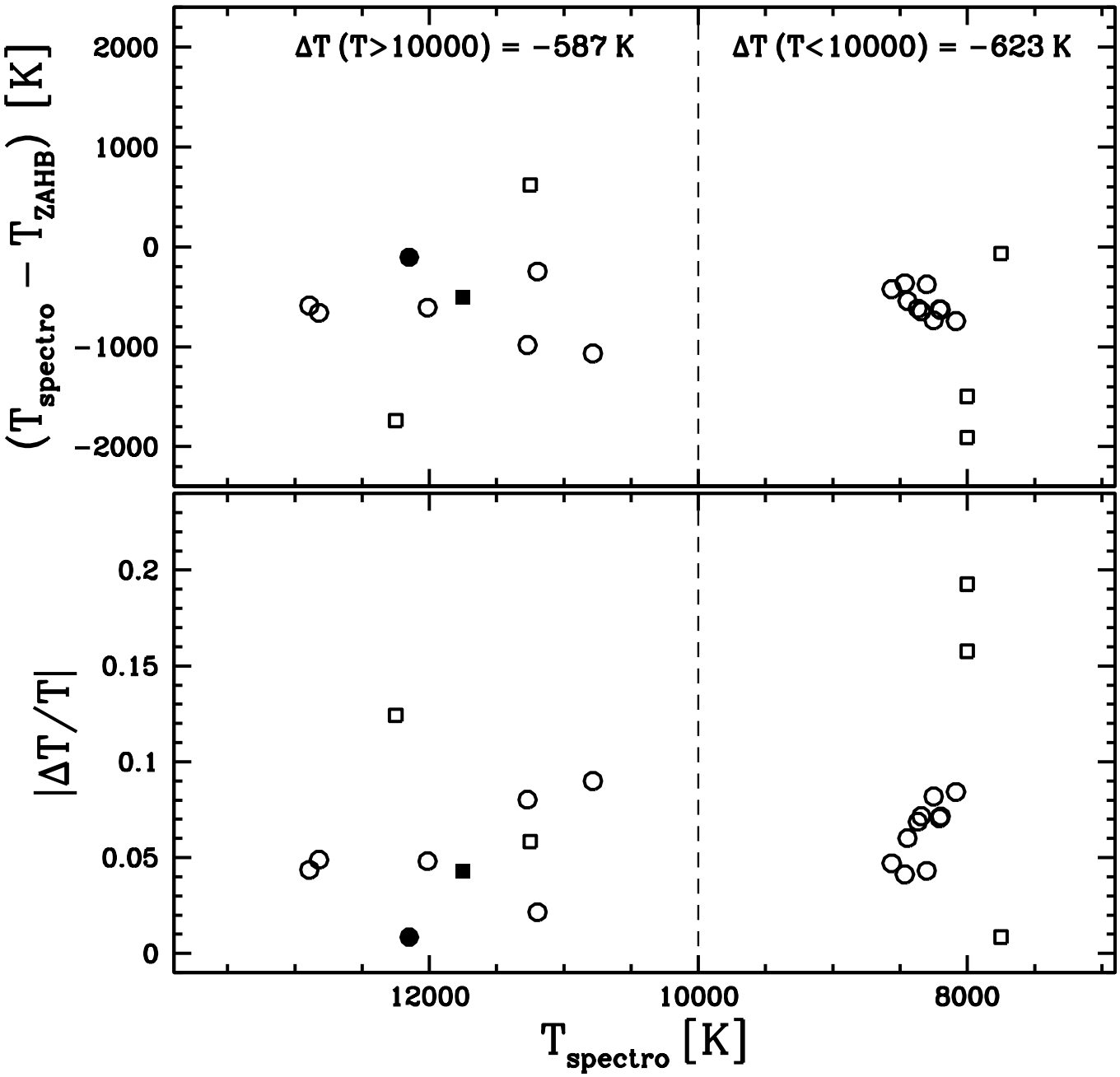

Figure 12. *Top*: Difference between spectroscopic ($T_{spectro}$) and photometric (T_{ZAHB}) temperature estimates for the HB stars in M15. Squares correspond to spectroscopic measurements of Möhler et al. (1995), circles to those of (Behr 2003). The filled symbols marks the only star (B348 in Buonanno et al. 1983) in common between the two samples. The median difference value for the stars with $T_{spectro} < 10,000$ K and $T_{spectro} > 10,000$ K are also labelled. *Bottom*: Absolute value of the relative temperature difference for the same stars.

Bragaglia, A., Carretta, E., Gratton, R., et al. 2010, A&A, 519, A60

Buonanno, R., Buscema, G., Corsi, C. E., Iannicola, G., & Fusi Pecci, F. 1983, A&AS, 51, 83

Buonanno, R., Corsi, C., Bellazzini, M., Ferraro, F. R., & Pecci, F. F. 1997, AJ, 113, 706

Castellani, M., & Tornambe, A. 1991, ApJ, 381, 393

Catelan, M. 2000, ApJ, 531, 826

Catelan, M. 2009, Ap&SS, 320, 261

Clement, C. M., Muzzin, A., Dufton, Q., et al. 2001, AJ, 122, 2587

Contreras Ramos, R., Ferraro, F. R., Dalessandro, E., Lanzoni, B., & Rood, R. T. 2012, ApJ, 748, 91

Corwin, T. M., Borissova, J., Stetson, P. B., et al. 2008, AJ, 135, 1459

Cutri, R. M., Skrutskie, M. F., van Dyk, S., et al. 2003, VizieR Online Data Catalog, 2246, 0

Dalessandro, E., Lanzoni, B., Ferraro, F. R., et al. 2008, ApJ, 677, 1069

Dalessandro, E., Beccari, G., Lanzoni, B., et al. 2009, ApJS, 182, 509

Dalessandro, E., Salaris, M., Ferraro, F. R., et al. 2011, MNRAS, 410, 694

Dalessandro, E., Schiavon, R. P., Rood, R. T., et al. 2012, AJ, 144, 126

Dalessandro, E., Salaris, M., Ferraro, F. R., Mucciarelli, A., & Cassisi, S. 2013, MNRAS, 430, 459
Dalessandro, E., Ferraro, F. R., Lanzoni, B., et al. 2013, ApJ, 770, 45
Dalessandro, E., Pallanca, C., Ferraro, F. R., et al. 2014, ApJ, 784, L29
D'Antona, F., Bellazzini, M., Caloi, V., et al. 2005, ApJ, 631, 868
Dolphin, A. E. 2009, PASP, 121, 655
Dorman, B., O'Connell, R. W., & Rood, R. T. 1995, ApJ, 442, 105
Dotter, A., Sarajedini, A., Anderson, J., et al. 2010, ApJ, 708, 698
Ferraro, F. R., Clementini, G., Fusi Pecci, F., & Buonanno, R. 1991, MNRAS, 252, 357
Ferraro, F. R., Fusi Pecci, F., & Buonanno, R. 1992, MNRAS, 256, 376
Ferraro, F. R., & Paresce, F. 1993, AJ, 106, 154
Ferraro, F. R., Paltrinieri, B., Fusi Pecci, F., et al. 1997, A&A, 324, 915
Ferraro, F. R., Paltrinieri, B., Fusi Pecci, F., et al. 1997, ApJ, 484, L145
Ferraro, F. R., Paltrinieri, B., Pecci, F. F., Rood, R. T., & Dorman, B. 1998, ApJ, 500, 311
Ferraro, F. R., D'Amico, N., Possenti, A., Mignani, R. P., & Paltrinieri, B. 2001, ApJ, 561, 337
Ferraro, F. R., Sills, A., Rood, R. T., Paltrinieri, B., & Buonanno, R. 2003, ApJ, 588, 464
Ferraro, F. R., Beccari, G., Dalessandro, E., et al. 2009, Nature, 462, 1028
Ferraro, F. R., Lanzoni, B., Dalessandro, E., et al. 2012, Nature, 492, 393
Freeman, K. C., & Norris, J. 1981, ARA&A, 19, 319
Fusi Pecci, F., Ferraro, F. R., Bellazzini, M., et al. 1993, AJ, 105, 1145
Girardi, L., Dalcanton, J., Williams, B., et al. 2008, PASP, 120, 583
Gratton, R. G., Carretta, E., Bragaglia, A., Lucatello, S., & D'Orazi, V. 2010, A&A, 517, A81
Greggio, L., & Renzini, A. 1990, ApJ, 364, 35
Harris, W. E. 1996, AJ, 112, 1487
Lagioia, E. P., Dalessandro, E., Ferraro, F. R., Lanzoni, B., & Salaris, M. 2014, arXiv:1402.0691
Lanzoni, B., Dalessandro, E., Ferraro, F. R., et al. 2007, ApJ, 663, 267
Lanzoni, B., Sanna, N., Ferraro, F. R., et al. 2007, ApJ, 663, 1040
Lanzoni, B., Dalessandro, E., Perina, S., et al. 2007, ApJ, 670, 1065
Lee, Y.-W., Demarque, P., & Zinn, R. 1994, ApJ, 423, 248
Lee, H.-c., Lee, Y.-W., & Gibson, B. K. 2002, AJ, 124, 2664
Milone, A. P., Marino, A. F., Dotter, A., et al. 2014, ApJ, 785, 21
Moehler, S., Heber, U., & de Boer, K. S. 1995, A&A, 294, 65
Möhler, S., Heber, U., & Durell, P. R. 1997, A&A, 317, L83
Möhler S., Sweigart A. V., Landsman W. B., Hammer N. J., Dreizler S. 2004, A&A, 415, 313
Moni Bidin, C., Villanova, S., Piotto, G., et al. 2012, A&A, 547, AA109
Origlia, L., Rood, R. T., Fabbri, S., et al. 2007, ApJ, 667, L85
Origlia, L., Ferraro, F. R., Fabbri, S., et al. 2014, A&A, 564, A136
Pace, G., Recio-Blanco, A., Piotto, G., & Momany, Y. 2006, A&A, 452, 493
Pasquini, L., Mauas, P., Käufl, H. U., & Cacciari, C. 2011, A&A, 531, A35
Pietrinferni, A., Cassisi, S., Salaris, M., & Castelli, F. 2006, ApJ, 642, 797
Piotto, G., Bedin, L. R., Anderson, J., et al. 2007, ApJ, 661, L53
Recio-Blanco, A., Aparicio, A., Piotto, G., de Angeli, F., & Djorgovski, S. G. 2006, A&A, 452, 875
Rich, R. M., Salim, S., Brinchmann, J., et al. 2005, ApJ, 619, L107
Roediger, J. C., Courteau, S., Graves, G., & Schiavon, R. P. 2014, ApJS, 210, 10
Rood, R. T., Beccari, G., Lanzoni, B., et al. 2008, Mem. Soc. Astron. Italiana, 79, 383
Salgado, C., Moni Bidin, C., Villanova, S., Geisler, D., & Catelan, M. 2013, A&A, 559, AA101
Sandage, A., & Wildey, R. 1967, ApJ, 150, 469
Sanna, N., Dalessandro, E., Lanzoni, B., et al. 2012, MNRAS, 422, 1171
Sanna, N., Dalessandro, E., Ferraro, F. R., et al. 2014, ApJ, 780, 90
Sarajedini, A., Bedin, L. R., Chaboyer, B., et al. 2007, AJ, 133, 1658
Schiavon, R. P., Dalessandro, E., Sohn, S. T., et al. 2012, AJ, 143, 121
Sohn, S. T., O'Connell, R. W., Kundu, A., et al. 2006, AJ, 131, 866
Stetson, P. B. 1987, PASP, 99, 191
Stetson, P. B. 1990, PASP, 102, 932
Stetson, P. B. 1993, IAU Colloq. 136: Stellar Photometry - Current Techniques and Future Developments, 291
Stetson, P. B. 1994, PASP, 106, 250
van den Bergh, S. 1967, AJ, 72, 70
Welch, G. A., & Code, A. D. 1972, Scientific results from the orbiting astronomical observatory (OAO-2), 310, 541

APPENDIX

A. CORRECTION FOR ZERO POINT VARIATION OF THE WFPC2 MOSAIC

As specified in the WFPC2 Data Handbook, the VEGAMAG zero points are referred to the last instrument calibration, which was performed as early as in 2002. Since the observations presented here were acquired in 2009 (7 years after) the calibrations could be out of date and could not provide anymore a precise calibration of each WFPC2 chip. In order to verify the validity of the adopted calibration we decided to plot different color-magnitude diagrams, using a different color code for stars belonging to the four different chips of the WFPC2 mosaic. In all of them we observed a clear misalignment of the evolutionary sequences both in color and magnitude. Therefore, we devised an empirical procedure for the re-alignment of the magnitudes of the four chips, using as reference the WF3 photometry as our reference catalog.

We started by fixing the F170W and the F555W magnitude displacements by re-aligning the RGB/AGB and HB sequences observed in the $(m_{\rm F170W}, m_{\rm F170W} - m_{\rm F555W})$ and $(m_{\rm F555W}, m_{\rm F170W} - m_{\rm F555W})$ CMDs (see Figure 13). Indeed, in these diagrams, the RGB/AGB sequence appears as an almost perfect vertical strip of stars, while the red HB appears as a sharp, diagonal sequence in the $(m_{\rm F170W}, m_{\rm F170W} - m_{\rm F555W})$ CMD and horizontal in the $(m_{\rm F555W}, m_{\rm F170W} - m_{\rm F555W})$ one (Lagioia et al. 2014). Hence we were able to determine the corrections to the adopted zero points in the F170W and F555W filters, by shifting in color and/or magnitude the RGB/AGB and HB sequences of the PC, WF2 and WF4 in order to match those obtained for the WF3 catalog.

After that, the displacement in $m_{\rm F255W}, m_{\rm F300W}, m_{\rm F336W}$ were straightforwardly recovered keeping the $m_{\rm F555W}$ shift fixed and assuming that the displacement observed in the $(m_i, m_i - m_{\rm F555W})$ CMD, with i = F255W, F300W, F336W, was entirely due to the i-th filter.

In the case of the F160BW magnitudes (because of the large calibration uncertainty) we adopted the best fit ZAHB model in the $(m_{\rm F160BW}, m_{\rm F160BW} - m_{\rm F555W})$ CMD as reference system and the magnitudes obtained for all the WFPC2 chips have bee reported to that reference.

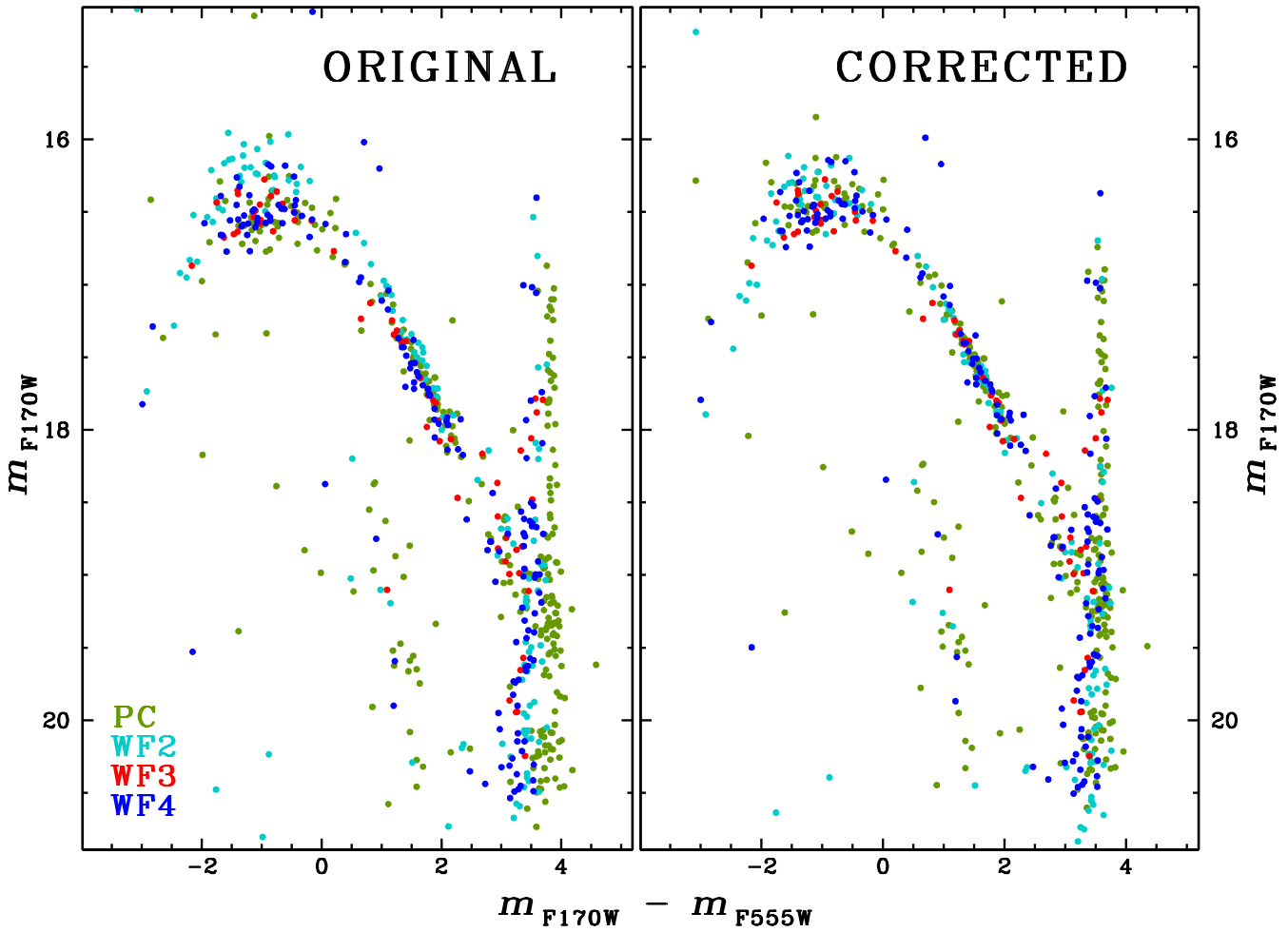

Figure 13. ($m_{\rm F170W}, m_{\rm F170W} - m_{\rm F555W}$) CMD of M15, showing with different colors the stars detected in the PC, WF2, WF3 and WF4 chips of WFPC2. *Left*: CMD obtained by adopting the zero points listed in the WFPC2 Data Handbook fot the calibration of instrumental magnitudes to the VEGAMAG system. *Right*: CMD obtained after the PC, WF2 and WF4 magnitudes were manually shifted to match the WF3 (red points) sequence.